FFEMS Fatigue & Fracture of Engineering Materials & Structures
ORIGINAL CONTRIBUTION
doi: 10.1111/ffe.12299

Analysis on the fatigue damage evolution of notched specimens with consideration of cyclic plasticity

F. SHEN[1], G. Z. VOYIADJIS[2], W. HU[1] and Q. MENG[1]

[1]*Institute of Solid Mechanics, School of Aeronautics Science and Engineering, Beihang University, Beijing 100191, China,* [2]*Department of Civil and Environmental Engineering, Louisiana State University, Baton Rouge, LA 70803, United States*

Received Date: 21 November 2014; Accepted Date: 23 February 2015; Published Online: 16 March 2015

ABSTRACT This paper presents a damage mechanics method applied successfully to assess fatigue life of notched specimens with plastic deformation at the notch tip. A damage-coupled elasto-plastic constitutive model is employed in which nonlinear kinematic hardening is considered. The accumulated damage is described by a stress-based damage model and a plastic strain-based damage model, which depend on the cyclic stress and accumulated plastic strain, respectively. A three-dimensional finite element implementation of these models is developed to predict the crack initiation life of notched specimens. Two cases, a notched plate under tension-compression loadings and an SAE notched shaft under bending-torsion loadings including non-proportional loadings, are studied and the predicted results are compared with experimental data.

Keywords continuum damage mechanics; cyclic plasticity; elasto-plastic; fatigue damage; fatigue life; notched specimens.

NOMENCLATURE

$\mathbf{D}$	= tensor damage variable
D	= scalar damage variable
S	= section area of the representative volume element
S_D	= total area of micro-cracks or micro-voids in the representative volume element
S_R	= effective area of resistance in the representative volume element
$\widetilde{\sigma}$	= effective stress
σ	= stress with damage
ε	= strain
ε_{ij}^{e}	= elastic strain
ε_{ij}^{p}	= plastic strain
E	= initial elastic modulus
v	= Poisson's ratio
α	= backstress
Q	= size of yield surface
$\dot{p}$	= accumulated plastic strain rate
$\dot{\lambda}$	= plastic multiplier
C_k, γ_k, b, Q_∞	= parameters of constitutive model
D_p	= plastic damage
$\sigma^*_{\max}$	= maximum value of the damage equivalent stress
S, m	= parameters of plastic strain-based damage model
D_e	= elastic damage
A_{II}	= amplitude of the octahedral shear stress
$\sigma_{H,mean}$	= mean value of the hydrostatic stress
$\sigma_{eq,\max}$	= maximum equivalent stress
σ_{l0}	= fatigue limit

Correspondence: F. Shen. E-mail: philshenfei@gmail.com

σ_u = ultimate tensile stress
a, M_0, β, b_1, b_2 = parameters of stress-based damage model
σ_y = initial yield stress
ε_f = fatigue ductility coefficient
c = fatigue ductility exponent

INTRODUCTION

Failure of machine components due to fatigue is of major concern in most engineering applications. The existence of a notch can lead to premature failure because of the concentration of stress. Experimental data of the high cycle fatigue (HCF) of notched specimens reveal the notch effect described by the fatigue notch factor K_f.[1] In some cases, stress at the notch tip exceeds the yield limit and plastic deformation occurs during the fatigue experiment, although the applied nominal stress is still below the yield limit. This study focuses on the prediction of fatigue life of notched specimens in these cases.

Two aspects about the fatigue life prediction of notched specimens are the stress analysis and the fatigue analysis, both of which were widely investigated in the last several decades. The stress analysis is to determine the local stress–strain history under the fatigue cyclic loading by the approximate method or the finite element (FE) method, as inputs to the fatigue analysis. The famous approximate methods are Neuber's rule[2] and subsequent equivalent strain energy density (ESED) method proposed by Glinka *et al.*[3] Ye *et al.*[4] developed a unified expression of elasto-plastic notch stress–strain calculation, of which Neuber's rule and the ESED method become two particular cases. By incorporating a cyclic plasticity model, the incremental form of the approximate method can achieve estimates with reasonable accuracy under complex external loading. Ince *et al.*[5] combined the ESED method and the Mroz plasticity model[6] to compute elasto-plastic stress–strain responses for notched components under non-proportional loading. However, due to the limitations of the approximate method, the FE method is inevitably employed to calculate the notch tip deformation. The FE analysis combined with cyclic plasticity model can provide reasonable local stress–strain for a notched member. Gao[7] compared the stress–strain results obtained by two approximate methods and the FE method for a notched shaft, and the results indicated the FE method associated with the cyclic plasticity model developed by Jiang and Sehitoglu[8,9] gave more accurate predictions for local deformations.

Numerous methods have been employed for the fatigue analysis of mechanical components. The direct use of stress or strain versus number of cycles to failure curves is the typical method for fatigue life prediction, which is convenient but confined to the application for some simple cases. The more sophisticated fatigue damage parameters, which can be stress, strain or energy,[10] are widely used to calculate fatigue life in the critical plane method for multiaxial fatigue. For example, the shear-stress range,[11] Smith–Watson–Topper[12,13] and Fatemi–Sociee[14,15] parameters have been studied for plain fatigue and fretting fatigue. There are two detailed procedures, local and non-local, for life prediction. Their use depends on whether the fatigue damage parameter is averaged over a line, an area or a volume. The local procedure calculates the local fatigue damage parameter and works well for unnotched specimens where the phenomenon of stress concentration does not occur. On the other hand, the non-local procedure can be used to address the fatigue life prediction of notched specimens. Krzyzak *et al.*[16] presented computational results using the non-local fatigue method, together with the volumetric approach, in which the energy parameter has been used to predict the fatigue life of notched elements. A unified fatigue criterion based on the critical plane concept was proposed by Jiang[17] for the analysis of fatigue crack initiation and growth. By using the criterion, the fatigue crack growth at the notch tip was investigated in the works of Jiang *et al.*[18,19] and Gao *et al.*,[20] in which the elasto-plastic stress–strain response was calculated by the robust cyclic plasticity model developed by Jiang and Sehitoglu.[8,9] Although the critical plane approaches mentioned earlier have gained widespread use, numbers of empirical fatigue damage parameters are employed, which reveals little about the characteristics of fatigue damage evolution.

The damage mechanics approach has been introduced to fatigue initiation problem, and it investigates the evolution of internal damage before macro-cracks become visible. The approach considers the mechanical behavior of a deteriorated medium on the macroscopic scale and evaluates progressive damage accumulated in the material until the damage reaches a critical value. Damage evolution law derived from thermodynamics is combined with a damage-coupled constitutive model of the material to simulate the evolution of the material damage. Xiao *et al.*[21] presented a continuum damage mechanics model for HCF and obtained good agreement between the predicted life and the experimental data. Marmi *et al.*[22] used an uncoupled damage mechanics approach with a non-local procedure to predict the fatigue life of tensile

samples with notches. Zhang *et al.*[23] developed a coupled damage mechanics approach in conjunction with FE analysis to predict plain and fretting fatigue life, and the results were compared with the critical plane method. The coupled damage mechanics approach is capable of capturing the material degradation, stress redistribution and the resulting effects on fatigue life. However, the effect of plasticity on the damage evolution has not been considered in the literature.[21–23]

To address the effect of plasticity in the framework of continuum damage mechanics, the damage-coupled elasto-plastic constitutive model is employed in this study, which incorporates the damage variable into the constitutive equations and therefore introduces a more rigorous description of the loss of load-carrying capacity. Voyiadjis and Kattan[24,25] proposed a coupled theory of anisotropic damage and finite strain plasticity in the Eulerian reference system and applied the model to the problem of finite simple shear. Voyiadjis *et al.*[26,27] incorporated the stress invariants into the coupled elasto-plastic constitutive model to investigate the ductile fracture. Kang *et al.*[28] used the damage-coupled visco-plastic constitutive model to study the uniaxial ratcheting and fatigue failure of tempered 42CrMo steel. Besides, it is also necessary to consider the effect of plasticity on the fatigue damage model. A simple damage model considering plastic strain is proposed by Lemaitre and Desmorat,[29] to address the low-cycle fatigue problem and is employed in this study.

The present work is concerned with fatigue crack initiation of notched specimens in the case that plastic deformation occurs at the notch tip. The effect of plasticity at the notch tip is considered in the continuum damage mechanics approach. Damage-coupled elasto-plastic constitutive model is employed to calculate the stress and strain of the damaged material. Two different fatigue damage models, a stress-based damage model and a plastic strain-based damage model, are adopted to calculate the damage increment induced by cyclic stress and accumulated plastic strain. The numerical implementation of these models is developed with the commercially available ABAQUS FE software to simulate the progressive damage accumulation of the material. Two cases, a notched plate under tension-compression loadings and an SAE notched shaft under bending-torsion loadings including non-proportional loadings, are studied by using the damage mechanics approach. The predicted results are compared with the experimental data.

THEORETICAL MODELS

Continuum damage mechanics was originally established by Kachanov.[30] A continuous damage variable was defined as a measurement of micro-cracks and micro-voids in the material. Following this work, continuum damage mechanics was extended to model fatigue, creep and ductile plastic damage. Lemaitre and Chaboche[31] presented some fundamental concepts in continuum damage mechanics, which are briefly described in this section for completeness.

Damage variable

Damage in its mechanical sense is the creation and growth of micro-cracks and/or micro-voids, which are discontinuities in a medium that is considered continuous at a larger scale. In engineering, the mechanics of continuous media can be described by a representative volume element in which all properties are represented by homogenized variables, as shown in Fig. 1.[32] The damage variable **D** associated with the direction of the normal vector $\vec{n}$ is defined as

$$D_n = \frac{S_D}{S} \tag{1}$$

where S is the area of a section of the RVE identified by its normal vector and S_D is the total area of micro-cracks or micro-voids, which constitute the damage. In this work, isotropic damage is assumed, in which case the damage tensor **D** is reduced to a scalar variable D

$$D = \frac{S - S_R}{S} \tag{2}$$

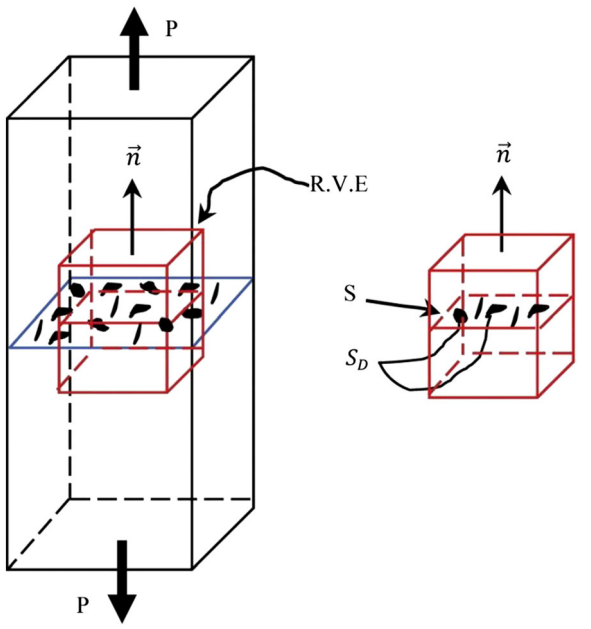

Fig. 1 Representative volume element.[32]

where S_R represents the effective area of resistance, $S_R = S - S_D = (1-D)S$. The effective stress $\tilde{\sigma}$ is introduced to describe stress over the section, which effectively resists the forces

$$\tilde{\sigma} = \frac{P}{S_R} = \frac{P}{(1-D)S} = \frac{\sigma}{1-D} \tag{3}$$

where P is the total load acting on the section with the area of S. The variable σ is the stress for the damaged material. Different definitions of damage can be found in the works of Voyiadjis *et al.*,[33,34] and the same equation as Eq. (3) is deduced based on the hypothesis of strain equivalence. Damage in the material is accumulated with increasing loading cycles. The initiation of macro-cracks takes place once the damage reaches a critical value. In this study, not all of the material in the notch section experiences plastic behavior. The critical value of accumulated damage is defined to be 1. At that moment, the effective area of resistance, S_R, reduces to zero and the effective stress $\tilde{\sigma}$ tends to infinity, which signals the initiation of macro-cracks.

The direct measurement of damage as the surface density of micro-cracks and/or micro-voids is difficult to perform, from a microscopic point of view. It is easier to measure damage by a macroscopic method. When plastic strain occurs, damage can be represented by the decrease of unloading elastic modulus after each cycle. Therefore, damage value is calculated by the unloading elastic modulus and the initial elastic modulus. However, this method is valid for uniform damage such as smooth specimen in the low-cycle fatigue. For notched specimen, damage is localized at the notch tip, and it is difficult to obtain the value of damage at the notch tip.

Damage-coupled elasto-plastic constitutive model

The Chaboche plasticity model[35–40] is used in this study because of the model's capability of describing the general cyclic deformation behavior and its comparative simplicity. With consideration of material damage, the damage variable is coupled into the Chaboche plasticity model by using the effective stress instead of the stress used in the elasticity law and in the Mises yield criterion, which is based on the hypothesis of strain equivalence.[31] The basic equations of the damage-coupled elasto-plastic constitutive model are listed as follows:

- The decomposition of total strain for small elastic strains

$$\varepsilon_{ij} = \varepsilon_{ij}^e + \varepsilon_{ij}^p \tag{4}$$

where ε_{ij}^e and ε_{ij}^p are the elastic strain and plastic strain, respectively. On the basis of the hypothesis of strain equivalence, the strains of undamaged material are the same with that of the damaged material.

- The elasticity law with damage is expressed as follows

$$\varepsilon_{ij}^e = \frac{1+v}{E}\left(\frac{\sigma_{ij}}{1-D}\right) - \frac{v}{E}\left(\frac{\sigma_{kk}\delta_{ij}}{1-D}\right) \tag{5}$$

where E and v are the elastic modulus and Poisson's ratio of the undamaged material, respectively. The variable σ_{ij} is the Cauchy stress of the damaged material.

- The yield function and plastic flow with damage is given as follows

$$F = \left(\frac{\sigma_{ij}}{1-D} - \alpha_{ij}\right)_{eq} - Q \tag{6}$$

$$\dot{\varepsilon}_{ij}^p = \dot{\lambda}\frac{\partial F}{\partial \sigma_{ij}} = \frac{3}{2}\frac{\dot{\lambda}}{1-D}\frac{\left(\frac{\sigma_{ij}}{1-D} - \alpha_{ij}\right)_{dev}}{\left(\frac{\sigma_{kl}}{1-D} - \alpha_{kl}\right)_{eq}} \tag{7}$$

$$\dot{p} = \sqrt{\frac{2}{3}\dot{\varepsilon}_{ij}^p \dot{\varepsilon}_{ij}^p} = \frac{\dot{\lambda}}{1-D} \tag{8}$$

The subscript 'dev' and 'eq' represent the deviatoric part of the stress and the Von Mises equivalent stress, respectively. The term α_{ij} is the deviatoric part of back stress, Q represents the size of the yield surface, $\dot{\lambda}$ is the plastic multiplier and $\dot{p}$ is the accumulated plastic strain rate.

- The hardening law with damage is expressed as follows

$$\dot{Q} = (1-D)\dot{p}b(Q_\infty - Q) \tag{9}$$

$$\alpha_{ij} = \sum_{k=1}^{M} \alpha_{ij}^{(k)} \tag{10}$$

$$\dot{\alpha}_{ij}^{(k)} = (1-D)\left(\frac{2}{3}C_k\dot{\varepsilon}_{ij}^p - \gamma_k \alpha_{ij}^{(k)}\dot{p}\right) \tag{11}$$

where M is the number of the back stress components. Parameters C_k, γ_k, b and Q_∞ are material constants determined from experimental tests.

Fatigue damage models

It is necessary to consider the damage induced by plastic strains when considering the plastic deformation at the notch tip. However, the materials which are not at the notch tip may experience elastic behavior. In this case, damage induced by cyclic stress also needs to be considered. In this study, two different damage laws are employed: a stress-based damage model and a plastic strain-based damage model,[41] which represent the evolution of damage in the material as the number of cycles

increases. Damage accumulates with increasing number of loading cycles until the value of damage reaches the critical value.

Plastic strain-based damage model

With the presence of macro-plastic strain, the corresponding damage accumulates over each fatigue cycle. The damage law,[31,41] which is dependent on the accumulated plastic strain, is given by

$$\frac{\mathrm{d}D_p}{\mathrm{d}N} = \left[\frac{\left(\sigma^*_{\max}\right)^2}{2ES(1-D)^2}\right]^m \Delta p \tag{12}$$

where $\sigma^*_{\max}$ is the maximum value of the damage equivalent stress[31] over a loading cycle. The parameters S and m are determined from the experimentally determined curve of plastic strain versus number of cycles to failure.

Stress-based damage model

A nonlinear fatigue damage model proposed by Lemaitre and Chaboche[31] for uniaxial fatigue is extended to the case of multiaxial fatigue by Chaudonneret.[42] The evolution of damage depends on stress quantities in one loading cycle and is written as follows:

$$\frac{\mathrm{d}D_e}{\mathrm{d}N} = \left[1-(1-D)^{\beta+1}\right]^{1-a\left\langle \frac{A_{II}-\sigma_{I0}\left(1-3b_1\sigma_{H,mean}\right)}{\sigma_u-\sigma_{eq,\max}}\right\rangle} \left[\frac{A_{II}}{M_0\left(1-3b_2\sigma_{H,mean}\right)(1-D)}\right]^{\beta} \tag{13}$$

where A_{II} and $\sigma_{H,mean}$ are the amplitude of the octahedral shear stress and the mean value of the hydrostatic stress in a loading cycle, respectively. The term $\sigma_{eq,\max}$ is the maximum equivalent stress over a loading cycle, σ_{I0} is the fatigue limit at the fully reversed loading condition and σ_u is the ultimate tensile stress. The details about the stress-based damage model can be obtained by referring to the literature.[22,23,31,42] The five parameters, a, M_0, β, b_1 and b_2, are determined by using plain fatigue tests of standard specimens.

MATERIAL PARAMETERS

In this research, three sets of material parameters need to be calibrated according to the experimental data. The methodology is illustrated briefly in the succeeding section.

Elasto-plastic constitutive model parameters

The experimental data of the uniaxial stress–strain curve are used for determining the material constants in the hardening law. The isotropic hardening is neglected in this study, which means the size of the yield surface remains unchanged

$$Q = \sigma_y \tag{14}$$

where σ_y is the initial yield stress. For the case of uniaxial loading, the stress–plastic strain relationship can be expressed as follows

$$\sigma = \sigma_y + \sum_{k=1}^{M} \frac{C_k}{\gamma_k}\left(1-e^{-\gamma_k\varepsilon_p}\right) \tag{15}$$

where σ and ε_p are stress and plastic strain, respectively. In this study, three components of back stress ($M = 3$) are employed to improve the accuracy of the data fitting. The least square method is employed to determine the parameters according to the experimental data.

Parameter identification for fatigue damage models

It is necessary to determine two sets of material parameters corresponding to two different fatigue damage models. In particular, experimental tests of high-cycle fatigue and low-cycle fatigue for unnotched specimens are employed to obtain these parameters.

Parameter identification for plastic strain-based damage model

The parameters in the plastic strain-based damage model are obtained by equating the integral of the damage evolution model, Eq. (12), with the curve of plastic strain versus number of cycles to failure. From the Coffin–Manson law, the equation for the plastic strain versus number of cycles to failure can be written as follows

$$\frac{\Delta\varepsilon_p}{2} = \varepsilon_f\left(2N_f\right)^c \tag{16}$$

where ε_f is the fatigue ductility coefficient and c is the fatigue ductility exponent. The integrated damage evolution equation for the case of uniaxial loading is found to be

$$N_F = \frac{1}{2(2m+1)\Delta\varepsilon_p}\left(\frac{2ES}{(\sigma_{\max})^2}\right)^m \tag{17}$$

The cyclic stress–strain curve is found as follows

$$\sigma_{\max} = K'\left(\frac{\Delta\varepsilon_p}{2}\right)^{n'} \tag{18}$$

where K' and n' are parameters obtained from experiments. Eq. (17) can then be written as follows

$$N_F = \frac{1}{2(2m+1)}\left(\frac{2^{1+2n'}ES}{(K')^2}\right)^m (\Delta\varepsilon_p)^{-(1+2mn')} \tag{19}$$

By comparing the two equations, the parameters S and m are determined according to the values of ε_f, c, K' and n'.

Parameter identification for the stress-based damage model

For uniaxial fatigue, the number of cycles to failure for a given stress condition is obtained by integrating Eq. (13) from $D=0$ to $D=1$, leading to the following

$$N_F = \frac{1}{1+\beta}\frac{1}{aM_0^{-\beta}}\frac{\langle\sigma_u - \sigma_{\max}\rangle}{\langle\sigma_a - \sigma_{l0}(1-b_1\sigma_m)\rangle}\left[\frac{\sigma_a}{1-b_2\sigma_m}\right]^{-\beta} \tag{20}$$

where $\sigma_{\max}$, σ_a and σ_m are the maximum stress, stress amplitude and mean stress during a loading cycle, respectively. The material parameters σ_{l0}, β and $aM_0^{-\beta}$ can be determined from a stress-controlled fatigue test at a fully reversed loading condition. The parameters b_1 and b_2 can be obtained from fatigue tests at different mean stresses. Parameter a is obtained according to the method introduced by Zhang.[23]

COMPUTATIONAL METHOD

The damage-coupled elasto-plastic constitutive model and fatigue damage models are implemented through the user subroutine UMAT in ABAQUS, which is called at all material integration points at the beginning of each time increment. The user subroutine updates the values of the stress and the solution-dependent state variables at the end of each time increment, which is followed by updating the corresponding Jacobian matrix. The central process in the procedure is the implementation of the implicit stress integration algorithm and determination of the evolution of the consistent elasto-plastic tangent modulus.[43–46] Because it is computationally expensive to simulate each loading cycle, the jump-in-cycles procedure is adopted in the numerical implementation, which assumes that stress, accumulated plastic strain and damage remain unchanged for a finite period of ΔN cycles constituting a block. With this assumption, the damage evolution can be interpreted as piecewise linear, with respect to the number of cycles. A simplified flowchart of the algorithm used in this study is shown in Fig. 2, and the details of the computational procedure are listed as follows:

(1) The initial damage for each element is set to be zero.
(2) The damage-coupled elasto-plastic constitutive rate equations, Eqs. (4)–(11), are solved to obtain the stress, elastic strain and plastic strain. The stress and accumulated plastic strain histories are calculated for the current block.
(3) According to the stress and accumulated plastic strain histories, two damage evolution rates can be calculated using two damage evolution equations, Eqs. (12) and (13). In the present work, the total damage evolution rate is assigned as the maximum value of two rates.[41]

$$\left(\frac{\mathrm{d}D}{\mathrm{d}N}\right)_j^i = \max\left\{\left(\frac{\mathrm{d}D_e}{\mathrm{d}N}\right)_j^i, \left(\frac{\mathrm{d}D_p}{\mathrm{d}N}\right)_j^i\right\} \tag{21}$$

where i represents the current block and j is the number of element.
(4) The damage values and the number of cycles for all elements are updated at the end of the current block. The determination of ΔN is necessary in order to obtain convergent fatigue life

$$D_j^{i+1} = D_j^i + \left(\frac{\mathrm{d}D}{\mathrm{d}N}\right)_j^i \Delta N \tag{22}$$

$$N^{i+1} = N^i + \Delta N \tag{23}$$

(5) Material properties are modified based on the calculated damage value for the next block, as given by

$$\text{Property}_j^{i+1} = \text{Property}\left(1 - D_j^{i+1}\right) \tag{24}$$

where 'Property' refers to the material parameters such as E, C_k, γ_k, and so on.
(6) The algorithm repeats steps (2)–(5) for each block of cycles until the damage value of any integration point reaches the critical value D_c. In this study, the critical value is set to 1.

STUDY CASES

Case 1. Notched plate under tension-compression loadings

A U-notched specimen made of LC4CS is investigated in this study, of which the elastic K_t value is

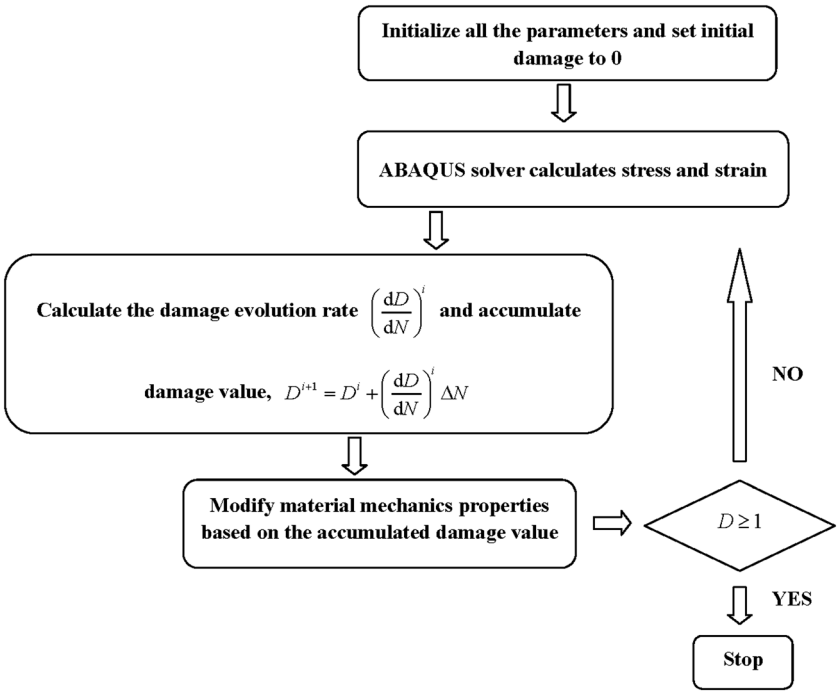

Fig. 2 Simplified flowchart of the computational method.

about 2. The shape of the specimen is based on the geometry from the literature,[47] as illustrated in Fig. 3. The plate thickness of all specimens is 2.5 mm. The specimens are subjected to the remote tension–compression or tension–tension fatigue loadings, as listed in Table 1. The material parameters for LC4CS are calibrated according to the necessary experimental data in the literature,[47] which are listed in Table 2. The result of data fitting for the plasticity model under the uniaxial loading is shown in Fig. 4a, and Fig. 4b depicts the fitting curves of the stress-based damage model for the fatigue experimental data of unnotched plate specimens.

The general purpose, nonlinear, FE code ABAQUS is used here. Only 1/8 of the specimen is modeled, and the symmetric boundary conditions are used at three planes of symmetry. The eight-node linear brick element C3D8 is employed in the present study, as shown in Fig. 5. A mesh convergence study is conducted by increasing the number of elements along the thickness direction. However, a negligible effect on the convergence results of stress is found with increasing refinement in the thickness direction.

The experiments with high stress condition are simulated by the continuum damage mechanics approach presented in this study, the crack initiation lives of which are below 100 000 cycles. The predicted fatigue lives are listed in Table 1 with experimental data, and the comparison is illustrated in Fig. 6. The bold line on the diagonal indicates a perfect agreement between the prediction and the experimentally observed crack initiation life, and the upper and lower lines on the same plot indicate the

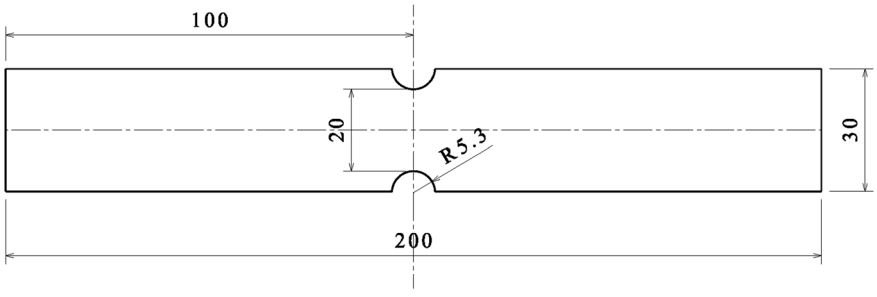

Fig. 3 Geometry of LC4CS specimens.

Table 1 Experimental data for LC4CS plate

No.	σ_{max} (MPa)	σ_{min} (MPa)	Experimental mean life (Cycles)	Predicted fatigue life (Cycles)
1	167	−167	17910	21300
2	127	−127	50040	41600
3	98	−98	86260	69600
4	226	−88	16250	17500
5	206	−68	24550	24400
6	177	−39	46420	38800
7	275	−1	16850	17000
8	245	29	35000	25600
9	216	58	68410	43200
10	324	88	16740	15800
11	314	98	19360	20000
12	284	128	50000	30000

σ_{max} and σ_{max} are the maximum and minimum stress of fatigue loading, respectively. The fatigue life given in the table is mean life of crack initiation.

Table 2 Material parameters for LC4CS

Constitutive model parameters:
$E = 73000$ MPa, $v = 0.33$, $\sigma_y = 433.8$ MPa, $C_1 = 1938.9$, $C_2 = 10712.3$, $C_3 = 102605.4$, $\gamma_1 = 16.88$, $\gamma_2 = 157$, $\gamma_3 = 1385.2$

Damage model parameters:
$S = 184.1$, $m = 0.5391$
$\sigma_u = 620$ MPa, $\sigma_{l0} = 72$ MPa, $\beta = 0.344$, $aM_0^{-\beta} = 7.373\text{e-}6$, $b_1 = 0.0017$, $b_2 = 0.0001$, $a = 0.75$

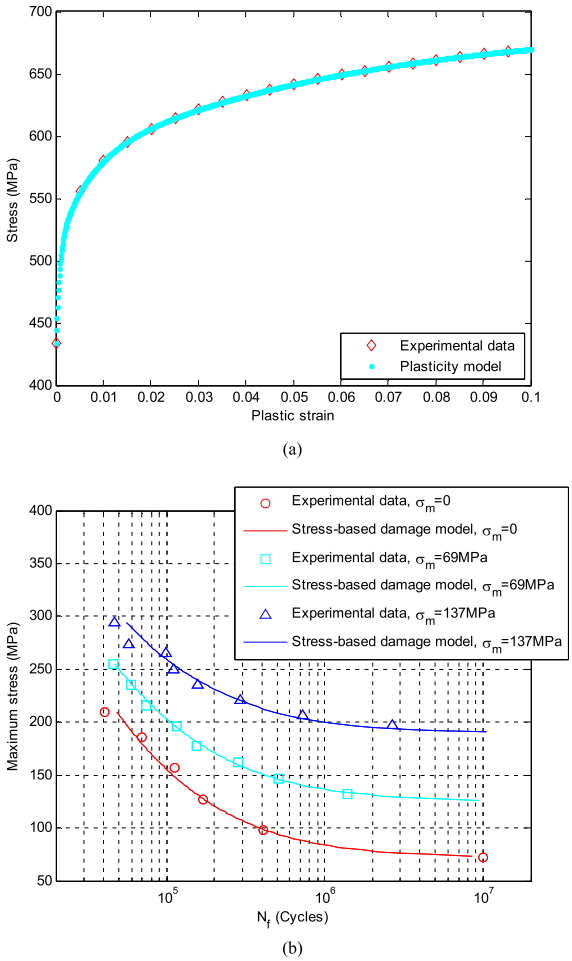

Fig. 4 Fitting curves of (a) the plasticity model under the uniaxial loading and (b) the stress-based damage model for the fatigue experimental data of the unnotched plate specimens for LC4CS.

borders of the deviations up to a factor of two. All the predictions fall within the factor of two scatter bands in the comparison figure.

For a notched specimen, the most critical element for crack initiation is at the notch tip due to the concentration of stress at this point. Besides, stress at the mid-thickness position is greater than that at the two edges of the notch tip along the thickness direction because of the Poisson effect at the notch tip. Figure 7 shows the contour of damage at the state of crack initiation under the fatigue loadings of experiment 1. The maximum damage occurs at the notch tip, and a similar result was reported by Zhang *et al.* and Oliveira Góes *et al.*[48] Therefore, we focus on the evolution of damage and the mechanical behavior of element 6404 as shown in Fig. 5. In the simulations, the remote compressive stress is not high enough to cause plastic deformation. No evident hysteresis loop is founded under cyclic tension-compression loading. If damage is not considered, plastic deformation will never occur again after the first loading cycle under constant amplitude loading. When considering damage, the damage variable involved in the yield equation accumulates with increasing number of loading cycles, which induces the yield function equals zero in the subsequent loading cycles when the value of the damage reaches a specific value. This is the plasticity induced by damage. Figure 8a shows the predicted evolution of the y direction stress–strain curve at one of the integration points in element 6404 under the fatigue loadings of $\sigma_{max} = 324$MPa and $\sigma_m = 206$MPa, and Fig. 8b depicts the curve for the first three blocks of the loading cycles. It is noted that there are 100 cycles in each block. One obvious phenomenon can be observed that the maximum stress reduces in each block of loading cycles as the number of loading cycles increases, the cause of which is the stress redistribution induced by damage. The damage in the material makes the stress and strain field near the notch tip to vary from cycle to cycle. It is also clear that the plastic strain range of element 6404 in the first block of the loading cycles is much greater than that in the subsequent blocks of loading cycles. The explanation is that the first plastic strain is directly caused by the local stress but the subsequent plastic

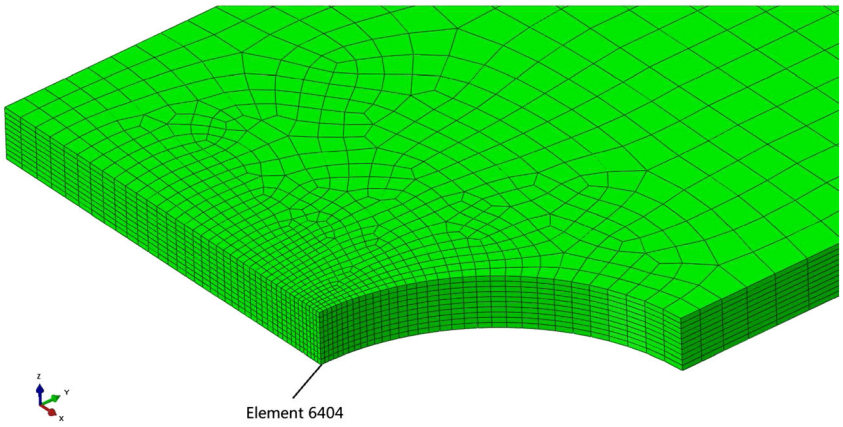

Fig. 5 One-eight of LC4CS specimen.

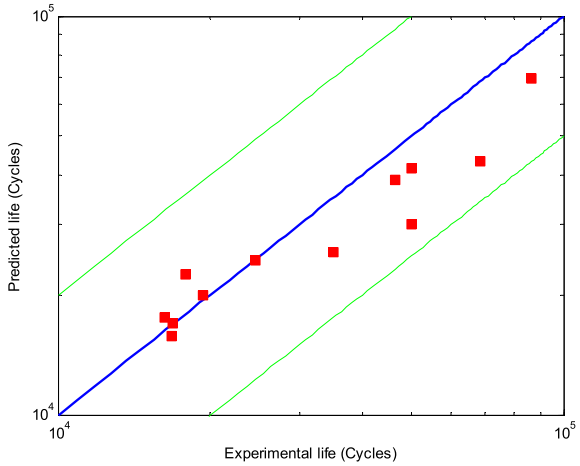

Fig. 6 Comparison of the predictions with experimental data for the LC4CS specimens.

strain is induced by coupling effect between damage and cyclic plasticity. Figure 9 shows the evolution of the damage rates calculated by two damage models for $\sigma_{\max} = 284$MPa, and $\sigma_m = 206$MPa. There is a sharp drop in the damage rate dD_p/dN during the first two blocks of loading cycles. The damage rate dD_p/dN is much smaller than dD_e/dN after the first block of loading cycles. If dD_p/dN is chosen to calculate the damage increment during all the loading cycles regardless of dD_e/dN, the predicted fatigue life will be greatly longer than the experimental life, resulting in serious deviation. Thus, the maximum one among the two damage rates is suitable to calculate the evolution of damage.

Case 2. SAE notched shaft under bending-torsion loadings

The damage mechanics method is applied to simulate the damage evolution of the SAE 1045 notched shaft under in-phase and out-of-phase bending-torsion loadings in the SAE test program.[49]

The whole shaft is modeled by three-dimensional high-order element C3D20 in ABAQUS to capture the stress concentration near the notch tip, as shown in Fig. 10. One end of the shaft is clamped, and the

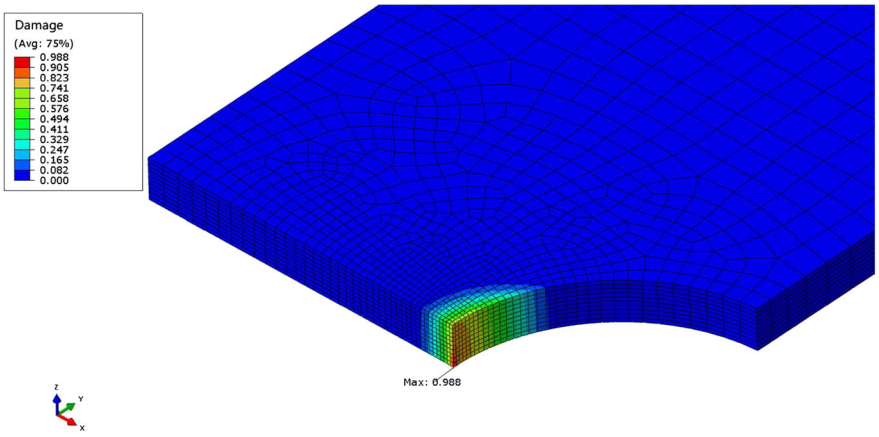

Fig. 7 Contour of damage at the state of the crack initiation under the fatigue loadings of experiment 1.

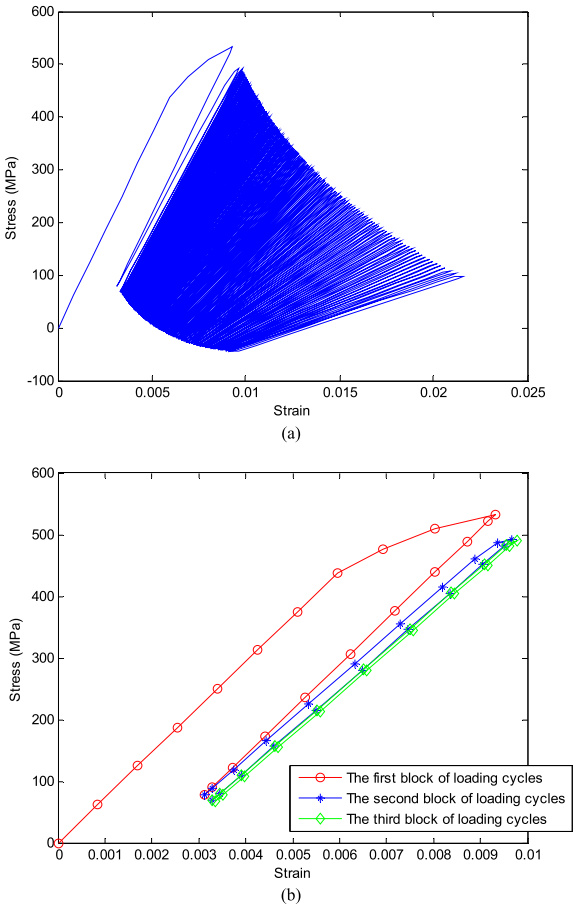

Fig. 8 Stress–strain curve evolution of element 882 for $\sigma_{max} = 324$ MPa, $\sigma_m = 206$ MPa. (a) for all of the blocks and (b) for the first three blocks.

bending-torsion loadings are applied by using the multi-point constraint method at the other end. A linear elastic FE analysis is conducted to determine the stress concentrations for bending and torsion loadings as $K_B = 1.6$ and $K_T = 1.3$ respectively, which agrees well with the experimental results.[50] It indicates the mesh size near the notch tip is appropriate.

The experiments with crack initiation life below 200 000 cycles are simulated by the damage mechanics method, as listed in Table 3. When the remote bending-torsion load is low, no plastic deformation occurs near the notch tip, which is beyond the focus of the present study.

For in-phase loadings

The cyclic stress–strain curve of normalized SAE 1045 steel is used to determine the parameters in the elasto-plastic constitutive model. All the parameters for normalized SAE 1045 steel are listed in Table 4.

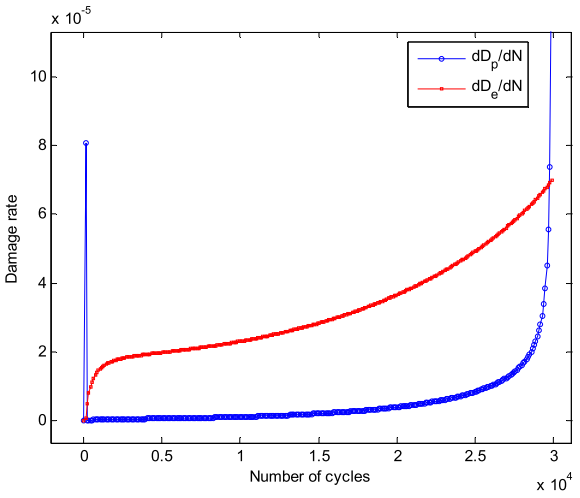

Fig. 9 Evolution of damage rates calculated by two damage models for $\sigma_{max} = 284$ MPa, $\sigma_m = 206$ MPa.

The predicted life is compared with the experimental crack initiation life, as shown in Fig. 11. The damage mechanics method provides reasonably accurate life predictions for the SAE notched shaft subjected to bending-torsion in-phase loadings, as most predictions fall within the factor of three scatter bands.

Figure 12 shows the predicted evolution of axial stress–strain curve for the most critical element at the fillet surface of the specimen RN-XR2-1. Obvious hysteresis loop is calculated because of the symmetric bending-torsion loadings. The maximum stress in each block of loading cycles reduces with the increasing loading cycles, which is similar to that in case 1. However, the plastic strain range increases. The two trends are both induced by damage, gradually changing the shape of the hysteresis loop. As mentioned in Section 5.1, the hysteresis loop will stabilize after several cycles without consideration of damage. Figure 13 shows the evolution of damage rates calculated by two damage models for the specimen RN-XR2-1. The two damage rates are comparable. The damage rate dD_p/dN is higher in the first one-third of the predicted fatigue life but lower than dD_e/dN in the remaining fatigue life. According to what is shown in Eq. (21) and Fig. 13, the damage rate increases slowly during the earlier stage of the predicted fatigue life and increases dramatically at the end. This trend is consistent with the change rate of the hysteresis loop.

For out-of-phase loadings

The damage mechanics method can be extended to cope with the cases of out-of-phase loadings. Two main changes in the damage mechanics method need to be considered because of the 90° out-of-phase loadings.

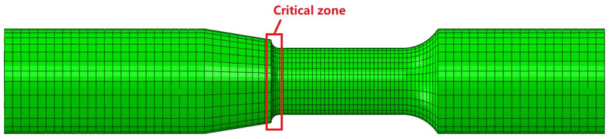

Fig. 10 Finite element model of the SAE notched shaft.

Table 3 Bending-torsion fatigue tests of SAE notched shaft specimen

Identification	Bending moment (N−m)	Torsion moment (N−m)	Phase angle (deg.)	Experimental life (Cycles)	Predicted life (Cycles)
JD-BR3-1	2800	0		2571	6000
IL-BR3-2	2600	0		3000	11000
AOS-BR3-1	2600	0		7930	11000
JD-BR3-2	2600	0		8111	11000
AOS-BR3-2	2586	0		14000	12000
JD-BR2-1	1875	0		41360	55000
BC-BR2-1	1875	0		55000	55000
RN-BR2-1	1730	0		30000	68000
IL-BR2-2	1730	0		49200	68000
IL-BR2-1	1730	0		60000	68000
AOS-BR2-1	1730	0		130000	68000
JD-TR3-1	0	3000		4057	8500
IL-TR3-1	0	3000		7000	8500
BC-TR3-1	0	2534		15000	14000
BC-TR2-1	0	2400		65000	55000
IL-TR2-1	0	2400		75700	55000
IL-XR3-1	1850	2550	0	2200	4700
RN-XR3-1	1850	2100	0	4780	11000
IL-XR3-3	1850	2100	0	6700	10200
IL-XR3-1	1355	2550	0	5500	11000
JD-XR3-1	2000	2100	0	5998	8500
RN-XR2-1	1220	1700	0	60800	65000
IL-XR2-1	1220	1710	0	72000	64000
JD-XR2-1	1220	1710	0	107500	64000
IL-YR2-1	1550	1090	0	80000	67500
IL-YR2-2	1550	1090	0	97500	67500
IL-YR3-1	2325	1350	0	2810	9100
IL-YR3-2	2325	1350	0	3000	9100
IL-YR3-1	1720	1350	0	17070	44500
IL-YR3-2	1720	1350	0	21450	44500
BC-YR2-1	1680	960	0	30000	56000
JD-YR2-2	1680	900	0	84950	60000
JD-YR2-1	1300	1400	0	84680	68000
IL-ZR3-1	1150	2700	0	3000	8650
JD-ZR3-1	1250	2700	0	6402	7650
IL-ZR3-1	851	2700	0	9000	13000
IL-ZR3-2	840	2700	0	10000	14000
IL-ZR2-1	780	2180	0	70000	52000
IL-ZR2-2	780	2180	0	70680	52000
IL-ZR2-3	570	2180	0	76100	57000
IL-ZR2-4	570	2180	0	99560	57000
JD-ZR03-1	1150	2700	90	10600	20000
JD-XR03-1	1850	2100	90	12660	30000
JD-XR03-2	1800	2100	90	21600	34000
BC-XR03-1	1698	2242	90	6725	41000
JD-YR03-1	2300	1325	90	17720	14000
JD-ZR03-2	770	2180	90	151900	70000
BC-XR03-2	1295	1710	90	25580	85000
JD-XR02-1	1220	1710	90	157500	90000
JD-XR02-2	1220	1710	90	173300	90000

Experimental life represents the fatigue life to 1.0 mm crack.

Table 4 Material parameters for SAE 1045 steel under in-phase loadings

Constitutive model parameters:
$E = 20400$ MPa, $v = 0.29$, $\sigma_y = 200$ MPa, $C_1 = 101268$, $C_2 = 11499$, $C_3 = 2772.64$, $\gamma_1 = 603.16$, $\gamma_2 = 57.745$, $\gamma_3 = 5.535$

Damage model parameters:
$S = 2.8895$, $m = 2.7113$
$\sigma_u = 624$ MPa, $\sigma_{l0} = 285$ MPa, $\beta = 0.0826$, $aM_0^{-\beta} = 3.1677\text{e-}5$, $b_1 = 0.0015$, $b_2 = 0.0002$, $a = 0.75$

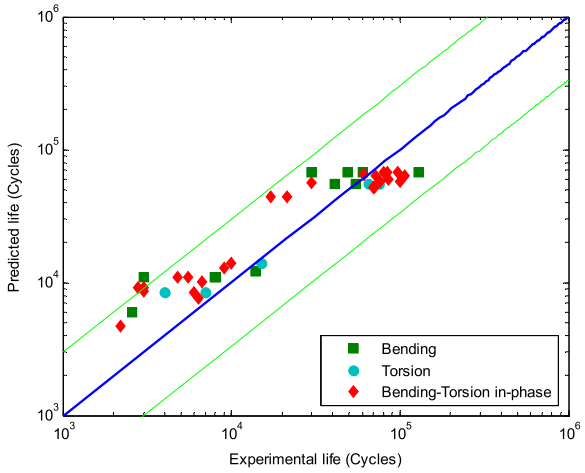

Fig. 11 Comparison of the predictions with experimental data for the SAE notched shaft under in-phase loadings.

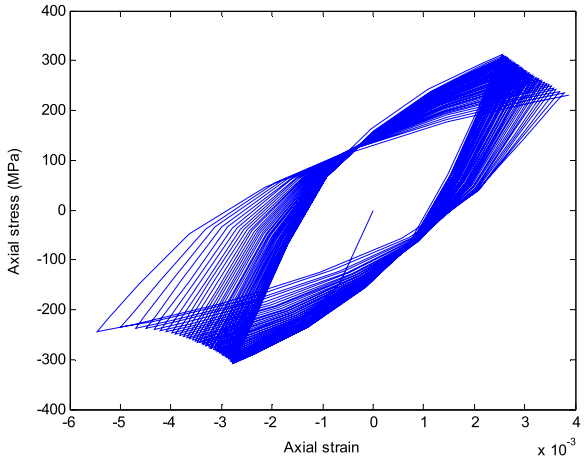

Fig. 12 Evolution of axial stress–strain curve for the most critical element in the specimen RN-XR2-1.

The first point is the non-proportional hardening of the normalized SAE 1045 steel under out-of-phase loading, which should be taken into account to obtain the accurate result of the stress and strain. As reported in the literature,[38,51] the Chaboche plasticity model is effective to address the non-proportional hardening.

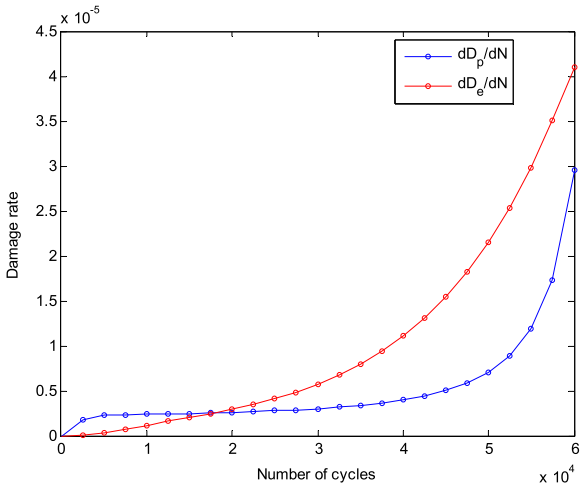

Fig. 13 Evolution of damage rates calculated by two damage models for the specimen RN-XR2-1.

Two improvements about the Chaboche plasticity model were proposed by Benallal *et al.* and Tanaka, both introducing non-proportional parameters in the plasticity model. In the present study, a simpler method is employed without changing the Chaboche plasticity model. The cyclic stress–strain curve under non-proportional loading was obtained experimentally and two parameters similar to K' and n' are determined.

$$K'_{90} = (1 + \alpha_{np})K' \qquad n'_{90} = n' \tag{25}$$

where α_{np} represents the non-proportional hardening coefficient. For normalized SAE 1045 steel, $\alpha_{np} = 0.3$ under the 90° out-of-phase loadings. Therefore, the parameters in the elasto-plastic constitutive model are obtained according to K'_{90} and n'_{90} for out-of-phase loadings, which are different from those under the in-phase loadings. All the parameters under the out-of-phase loadings are listed in Table 5, in which the parameters for the two damage models are unchanged.

The second point is the calculation of $\sigma^*_{\max}$ in the plastic strain-based damage model and A_{II}, $\sigma_{eq,\max}$ in the

Table 5 Material parameters for SAE 1045 steel under out-of-phase loadings

Constitutive model parameters:
$E = 20400$ MPa, $v = 0.29$, $\sigma_y = 200$ MPa, $C_1 = 256340$, $C_2 = 18364$, $C_3 = 3857.1$, $\gamma_1 = 1018.3$, $\gamma_2 = 67.8955$, $\gamma_3 = 5.9468$

Damage model parameters:
$S = 2.8895$, $m = 2.7113$
$\sigma_u = 624$ MPa, $\sigma_{l0} = 285$ MPa, $\beta = 0.0826$, $aM_0^{-\beta} = 3.1677\text{e-}5$, $b_1 = 0.0015$, $b_2 = 0.0002$, $a = 0.75$

stress-based damage model under out-of-phase loading. Because it is unable to know in advance when the stress quantities $\sigma^*_{\max}$ and $\sigma_{eq,\max}$ occur in a loading cycle directly, the quantities at the time increments during one loading cycle are compared with each other and the maximum one is picked. For non-proportional loading, the calculation of A_{II} is defined as follows

$$A_{II} = \frac{1}{2}\max_{t}\max_{t_0}\left[\frac{3}{2}\left(s_{ij,t} - s_{ij,t_0}\right)\left(s_{ij,t} - s_{ij,t_0}\right)\right]^{1/2} \tag{26}$$

where $s_{ij,t}$ and s_{ij,t_0} represent the deviatoric stress tensor components at the time increment t and t_0 in a loading cycle, respectively.

Figure 14 shows the histories of the stress components and equivalent stress for the most critical element in the specimen JD-ZR03-1 during the first block of loading cycles. The axial and hoop stresses, σ_{22} and σ_{12}, are predominant compared with the four other components as shown in Fig. 14, which relates to the remote bending and torsion loadings respectively. For this specimen, the stress quantities, $\sigma^*_{\max}$ and $\sigma_{eq,\max}$, are determined at the time increment of three-fourth cycle, and A_{II} is calculated based on the stress components at the two critical time increments. As the bending-torsion loading changes, these critical time increments also vary, as shown in Fig. 15.

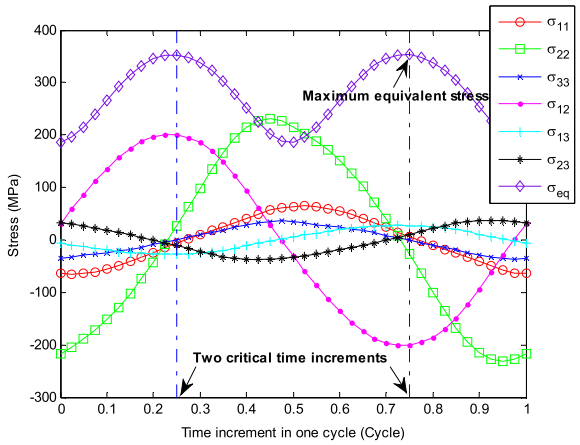

Fig. 14 Histories of stress components and equivalent stress for the most critical element in the specimen JD-ZR03-1 during the first block of loading cycles.

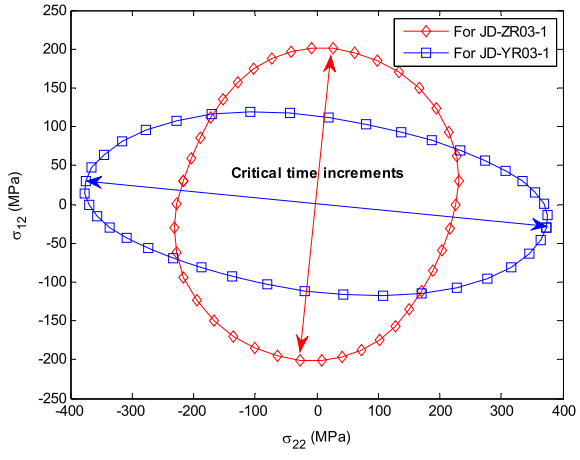

Fig. 15 Relationships between σ_{22} and σ_{12} for the most critical element in two specimens.

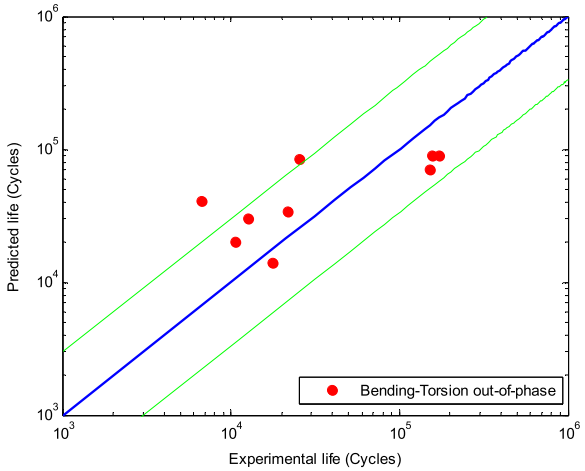

Fig. 16 Comparison of the predictions with experimental data for the SAE notched shaft under out-of-phase loadings.

Figure 16 depicts the prediction capability of the damage mechanics method in estimating the crack initiation life under the 90° out-of-phase loadings. With consideration of the large scatter in experimental data, the method provides reasonable predictions.

CONCLUSIONS

In the present study, a damage mechanics approach is developed to predict fatigue crack initiation life of notched specimens. The elasto-plastic behavior of the material at the notch tip is considered, and the damage is calculated by two fatigue damage models: a stress-based damage model and a plastic strain-based damage model. These models are implemented in ABAQUS and the two cases including tension-compression, bending-torsion, in-phase and out-of phase loadings are studied. The predicted fatigue lives are compared with the experimental results. Several features of the damage mechanics approach in this study can be concluded as follows:

- A damage-coupled elasto-plastic constitutive model is employed to represent the elasto-plastic behavior of a material with damage at the notch tip.
- A rule of damage accumulation is proposed for the case of material experiencing elasto-plastic deformation. The predicted results agree well with the experimental data.

- The evolutions of the mechanical behavior of the material, such as the stress–strain relationship and the relation between damage accumulation and loading cycles, are revealed by the damage mechanics approach, which would contribute to the understanding and calculation of the fatigue damage in material.
- The extended approach to the fatigue under non-proportional loading is proposed, in which non-proportional hardening and a new calculation of stress quantities are considered. The predicted results agree well with the experimental data.

Acknowledgements

Financial support by National Natural Science Foundation of China (11002010) is gratefully acknowledged.

REFERENCES

1 Suresh S. (1998) Fatigue of Materials. Cambridge University Press, Cambridge.
2 Neuber H. (1961) Theory of stress concentration for shear-strained prismatic bodies with arbitrary nonlinear stress–strain laws. *J. Appl. Mech.*, **28**, 544–550.
3 Molski K., Glinka C. (1981) A method of elastic–plastic stress and strain calculation at a notch root. *Mater. Sci. Eng.*, **60**, 93–100.
4 Ye D. Y., Hertel O., Vormwald M. (2008) A unified expression of elastic–plastic notch stress–strain calculation in bodies subjected to multiaxial cyclic loading. *Int. J. Solids Struct.*, **45**, 6177–6189.
5 Ince A., Glinka G., Buczynski A. (2014) Computational modeling of multiaxial elasto-plastic stress–strain response for notched components under non-proportional loading. *Int. J. Fatigue*, **62**, 42–52.
6 Mroz Z. (1967). On the description of anisotropic work hardening. *J. Mech. Phys. Solids*, **15**, 163–175.
7 Gao Z., Qiu B., Xiaogui W., Jiang Y. (2010) An investigation of fatigue of a notched member. *Int. J. Fatigue*, **32**, 1960–1969.
8 Jiang Y, Sehitoglu H. (1996) Modeling of cyclic ratchetting plasticity. Part I – development of constitutive equations. *J. Appl. Mech.*, **63**, 720–725.
9 Jiang Y, Sehitoglu H. (1996) Modeling of cyclic ratchetting plasticity. Part II – implement of the new model and comparison of theory with experiments. *J. Appl. Mech.*, **63**, 726–733.
10 Karolczuk A., Macha E. (2005) A review of critical plane orientations in multiaxial fatigue failure criteria of metallic materials. *Int. J. Fract.*, **134**, 267–304.
11 Naboulsi S., Mall S. (2003) Fretting fatigue crack initiation behavior using process volume approach and finite element analysis. *Tribol. Int.*, **36**, 121–131.
12 Smith K. N., Watson P, Topper T. H. (1970) A stress–strain function for the fatigue of metals. *J. Mater.*, **15**, 767–778.
13 Szolwinski M. P., Farris T. N. (1996) Mechanics of fretting fatigue crack formation. *Wear*, **198**, 93–107.
14 Fatemi A., Socie D. F. (1988) A critical plane approach to multiaxial fatigue damage including out-of-phase loading. *Fatigue Fract. Engng. Mater. Struct.*, **11**, 149–165.
15 Lykins C. D., Mall S., Jain V. (2000) An evaluation of parameters for fretting fatigue crack initiation. *Int. J. Fatigue*, **22**, 703–716.
16 Krzyzak D., Lagoda T. (2014) Fatigue life estimation of notched elements with non-local volumetric method. *Int. J. fatigue*, **61**, 59–66.
17 Jiang, Y. (2000) A fatigue criterion for general multiaxial loading. *Fatigue Fract. Engng. Mater. Struct.*, **23**, 19–32.
18 Ding F., Feng M., Jiang Y. (2007) Modeling of fatigue crack growth from a notch. *Int. J. Plast.*, **23**, 1167–1188.
19 Fan F., Kalnaus S., Jiang Y. (2008) Modeling of fatigue crack growth of stainless steel 304L. *Mech. Mater.*, **40**, 961–973.
20 Wang X., Yin D., Feng X., Qiu B., Gao Z. (2012) Fatigue crack initiation and growth of 16MnR steel with stress ratio effects. *Int. J. Fatigue*, **35**, 10–15.
21 Xiao Y. C., Li S., Gao Z. (1998) A continuum damage mechanics model for high cycle fatigue. *Int. J. Fatigue*, **20**, 503–508.
22 Marmi A. K., Habraken A. M., Duchene L. (2009) Multiaxial fatigue damage modeling at macro scale of Ti-6Al-4V alloy. *Int. J. Fatigue*, **31**, 2031–2040.
23 Zhang T., McHugh P. E., Leen S. B. (2012) Finite element implementation of multiaxial continuum damage mechanics for plain and fretting fatigue. *Int. J. Fatigue*, **44**, 260–272.
24 Voyiadjis G. Z., Kattan P. I. (1992) A plasticity-damage theory for large deformation of solids - I. Theoretical formulation. *Int. J. Engng. Sci.*, **30**, 1089–1108.
25 Kattan P. I., Voyiadjis G. Z. (1993) A plasticity-damage theory for large deformation of solids - II. Applications to finite simple shear. *Int. J. Engng. Sci.*, **31**, 183–199.
26 Voyiadjis G. Z., Hoseini S. H., Farrahi G. H. (2012) Effects of stress invariants and reverse loading on ductile fracture initiation. *Int. J. Solids Struct.*, **29**, 1541–1556.
27 Voyiadjis G. Z., Hoseini S. H., Farrahi G. H. (2012) A plasticity model for metals with dependency on all the stress invariants. *J. Eng. Mater. Technol.*, **135**, 011002–13.
28 Kang G. Z., Liu Y. J., Ding J., Gao Q. (2009) Uniaxial ratcheting and fatigue failure of tempered 42CrMo steel: Damage evolution and damage-coupled visco-plastic constitutive model. *Int. J. Plast.*, **25**, 838–860.
29 Lemaitre J., Rodrigue D. (2005) Engineering Damage Mechanics. Springer, Berlin.
30 Kachanov L. M (1958) Time of the rupture process under creep conditions. *Izv Akad Nauk SSR Otd Tech Nauk*, **8**, 26–31.
31 Lemaitre J., Chaboche J. L. (1994) Mechanics of Solid Materials. Cambridge University Press, Cambridge.
32 Hojjati-Talemi R., Wahab Magd Abdel. (2013) Fretting fatigue crack initiation lifetime predictor: using damage mechanics approach. *Tribol. Int.*, **60**, 176–186.
33 Voyiadjis G. Z., Kattan P. I. (2009) A comparative study of damage variables in continuum damage mechanics. *Int. J. Damage Mech.*, **18**, 315–340.
34 Voyiadjis G. Z., Kattan P. I. (2012) Mechanics of damage processes in series and in parallel: a conceptual framework. *Acta Mech.*, **223**, 1863–1878.
35 Chaboche J. L. (1986) Time-independent constitutive theories for cyclic plasticity. *Int. J. Plast.*, **2**, 149–188.
36 Chaboche J. L. (1989) Constitutive equations for cyclic plasticity and cyclic viscoplasticity. *Int. J. Plast.*, **5**, 247–302.
37 Chaboche J. L. (1991) On some modifications of kinematic hardening to improve the description of ratcheting effects. *Int. J. Plast.*, **7**, 661–678.
38 Chaboche J. L. (2008) A review of some plasticity and viscoplasticity constitutive theories. *Int. J. Plast.*, **24**, 1642–1693.
39 Abdel-Karim M. (2009) Modified kinematic hardening rules for simulations of ratchetting. *Int. J. Plast.*, **25**, 1560–1687.

40 Abdel-Karim M. (2010) An evaluation for several kinematic hardening rules on prediction of multiaxial stress-controlled ratchetting. *Int. J. Plast.*, **26**, 711–730.
41 Warhadpande A., Sadeghi F, Michael N. K., Doll G. (2012) Effects of plasticity on subsurface initiated spalling in rolling contact fatigue. *Int. J. Fatigue*, **36**, 80–95.
42 Chaudonneret M. (1993) A simple and efficient multiaxial fatigue damage model for engineering application of macrocrack initiation. *J. Engng. Mater. Technol.*, **115**, 373–379.
43 Simo J. C., Taylor R. L. (1985) Consistent tangent operator for rate-independent elastoplasticity. *Comput. Method App. M.*, **48**. 101–118.
44 Kang G. Z. (2004) A visco-plastic constitutive model for ratcheting of cyclically stable materials and its finite element implementation. *Mech. Mater.*, **36**, 299–312.
45 Kang G. Z. (2008) Ratchetting: Recent progresses in phenomenon observation, constitutive modeling and application. *Int. J. Fatigue*, **30**, 1448–1472.
46 Belytschko T., Liu W. K., Moran B. (2000) Nonlinear Finite Elements for Continua and Structures. Wiley, Chichester.
47 Wu X. R. (1997) Handbook of Mechanics Properties of Aircraft Structure Metals. Aviation Industry Press, Beijing.
48 de Oliveira Góes R. C., de Castro J. T. P., Martha L. F. (2014) 3D effects around notch and crack tips. *Int. J. Fatigue*, **62**, 159–170.
49 G. E. Leese, D. Socie (Eds.), (1989) *Multiaxial Fatigue*: *Analysis and Experiments* (SAE-AE-14), Society of Automotive Engineers, Warrendale, PA.
50 Ince A., Glinka G. (2014) A generalized fatigue damage parameter for multiaxial fatigue life prediction under proportional and non-proportional loadings. *Int. J. Fatigue*, **62**, 34–41.
51 Benallal A., Marquis D. (1987) Constitutive equations for nonproportional cyclic elasto-viscoplasticity. *J. Engng. Mater. Technol.*, **109**, 326–336.